Instabilities across the Scales: Simple Models for Shear Banding, Plate Subduction and Mantle Convection in Geodynamics

Hans-Bernd Mühlhaus[1,2], Louis Moresi[3], Matt Davies[1], Klaus Gottschald[1], and Alina Hale[4]

[1] Earth Systems Science Computational Centre (ESSCC),
   The University of Queensland, St Lucia, Queensland, Australia
   `muhlhaus@uq.edu`
[2] CSIRO Division of Exploration and Mining, 26 Dick Perry Ave, Kensington,
   Western Australia, Australia
[3] School of Mathematical Sciences, Monash University, Clayton, Victoria,
   Australia
[4] School of Geosciences, University of Sydney, Sydney, Australia

Abstract. The Earth shows different modes of deformation in response to thermal or gravitational driving forces. The bulk mantle convects like a viscous fluid on the global scale, while the lithosphere is broken into several plates. They show little internal deformation, but change their shapes and relative positions. Oceanic plate material is generated at divergent margins and recycled into the mantle at subduction zones, on a regional scale. The buoyant continental crust resists subduction and develops meter-scale shear bands during deformation.

In this article we review Eulerian finite element (FE) schemes and a particle-in-cell (PIC) FE scheme [15]. Focussing initially on models of crustal deformation at a scale of a few tens of km, we choose a Mohr-Coulomb yield criterion based upon the idea that frictional slip occurs on whichever one of many randomly oriented planes happens to be favourably oriented with respect to the stress field. As coupled crust/mantle models become more sophisticated it is important to be able to use whichever failure model is appropriate to a given part of the system. We have therefore developed a way to represent Mohr-Coulomb failure within a mantle-convection fluid dynamics code.

With the modelling of lithosphere deformation we use an orthotropic viscous rheology (a different viscosity for pure shear to that for simple shear) to define a preferred plane for slip to occur given the local stress field. The simple-shear viscosity and the deformation can then be iterated to ensure

that the yield criterion is always satisfied. We again assume the Boussinesq approximation - neglecting any effect of dilatancy on the stress field.

Subduction is modelled as a Rayleigh-Taylor instability with dense oceanic lithosphere sinking into less dense sublithospheric mantle. We use a linear viscous rheology for the mantle in this case. Parts of the lithosphere are viscous, others brittle. The values of the dynamic viscosity are different for lithosphere and mantle. The brittle behaviour of parts of the lithosphere can be modelled in the continuum limit by using a viscoplastic rheology.

Turning to the largest planetary scale, we present an outline of the mechanics of unified models plate-mantle models and then show how computational solutions can be obtained for such models using Escript. The consequent results for different types of convection are presented and the stability of the observed flow patterns with respect to different initial conditions and computational resolutions is discussed.

1   Introduction

Heat loss from the Earth's deep interior occurs through a process of thermal convection in the solid mantle. The pattern of deep convection is not directly observable as it is strongly modified by the very non-linear response of the near-surface rocks in the cool thermal boundary layer (the lithosphere).

The ocean floor is made up of a dozen or so near-rigid "plates" which constitute the upper thermal boundary layer of this convection system. Consequently, the entire ocean floor is recycled with a characteristic time of 100-200 million years.

Tectonic plates on Earth are characterized by little internal deformation , but changing relative positions and shapes due to subduction, deformation in back-arc basins or collisional zones, and generation of oceanic lithosphere, all at different plate rim segments. This mode of convection is the primary means of cooling the mantle, mainly driven by the negative buoyancy of subducting slabs.

The entire ocean floor is recycled with a characteristic time of 100-200 million years. Continents do not participate in the active overturn of the mantle, largely because they contain a high percentage of granitic rock which is light relative to the olivine composition of the mantle. The continents have been able to resist being recycled completely for at least 4 billion years. In some areas ("cratons") have remained largely undeformed for this time, while other areas have undergone enormous deformation to form (and reform) mountain belts. The strong correlation between seismicity and plate boundaries (e.g. Barazangi and Dorman) makes it seem likely that plate motions are associated with localization of deformation occurring when stresses reach the yield strength of the lithosphere. In addition, close to the surface where temperatures are less than approximately $600°$ C it becomes necessary to consider the role of elasticity.

From a modelling point of view, it is necessary to consider the fluid convection of the mantle and the history-dependent viscoelastic/brittle behaviour of the continental crust as a single coupled system. The requirements for a geological simulation code are therefore an ability to track boundaries and interfaces through extremely large deformation, including fluid convection, of non-linear history dependent materials. The wide range of physical and temporal scales, and the many coupled physical processes also impose a need for computational efficiency. The code should also be very flexible in the rheological laws which it can treat.

In this paper we describe two flow models which accurately treat these difficulties at overlapping scales. In the first we describe an orthotropic plasticity model formulated from a fluid dynamics viewpoint which can model coupled mantle convection and crustal deformation. This model can also be used to model localized faulting in the crust. In the second example, we examine the role of the temperature-dependent viscosity and elasticity in planetary scale convection models with a yield criterion applied to the lithosphere.

1.1   *Continuum Deformation and Fault Formation*

The surface deformation of the Earth is dominated by the presence of faults on which a very large fraction of strain is accommodated in the long term (Dolan, *pers. comm.*). In the modeling of large scale deformation of the Earth in both the ocean basins and in the continents, there has been a strong philosophical divide between those who consider that these faults are dominant, fundamentally distinct, component of the system at every scale [28, 30, 29, 31, 32, 2], and those who believe that, on a lithospheric scale, the deformation on faults can be averaged within a continuum description more in tune with the underlying driving forces [7, 8].

The reason that such a debate is possible after many years of discussion is almost certainly due to the fact that each of these approaches captures something important, but different, about the way the Earth works. In models of actively deforming continents, a thin skin continuum representation of the mantle lithosphere and crust captures the large-scale deformation in a reliable, reproducible way [6, 7] but not capture important detail in the surface strain field associated with the largest faults. Thin skin models of the brittle layer in which known faults are explicitly included capture this fine detail [2, 14] but the fidelity of the model deformation is very reliant on accurate prior knowledge of the faults' distribution and their dips.

A "thick-skin" model of the continental lithosphere which also includes the major faults in the brittle regime is the appropriate way to bridge these two thin-skin approaches, but is significantly more challenging computationally. We describe an algorithm which can model both the frictional behaviour of localized faults, the non-linear rheology applicable to the broad scale where the faults are too small to resolve individually, and the fluid behaviour of active thermal convection in the mantle.

We use a linear viscous rheology for the mantle. Parts of the lithosphere are viscous, others brittle. The values of the dynamic viscosity are different for lithosphere and mantle. In regional subduction models, the brittle behaviour of parts of the lithosphere can be modelled in the continuum limit by using the viscoplastic rheology. Elastoviscoplastic deformation is a more suitable description for the small scale behaviour of the crust.

2 Constitutive Models

In geodynamics we commonly treat the Earth on a large scale as an incompressible, viscous fluid with infinite Prandtl number in which motions are driven by internal temperature variations. Elastic deformation is important only in the low-temperature part of the system and is therefore usually assumed to have a minor effect on the system at the largest (planetary) scale [26, 27]. The force term is a gravitational body force due to density changes. We assume that these arise, for any given material, through temperature effects so that:

$$\sigma_{ij,j} - p_{,i} = g\rho_0(1 - \alpha_T T)z_i \tag{1}$$

where g is the acceleration due to gravity, ρ_0 is material density at a reference temperature, α_T is the coefficient of thermal expansivity, and T is temperature. z_i is a unit vector in the vertical direction. We have also assumed that the variation in density only needs to be considered in the driving term (the Boussinesq approximation: Boussinesq, 1903).

Substituting a general viscous constitutive law

$$\sigma_{ij} = 2\eta_{ijkl}D_{kl}, \qquad D_{ij} = (v_{i,j} + v_{j,i})/2 \tag{2}$$

gives the equation of motion:

$$(\eta_{ijkl}D_{kl})_{,j} - p_{,i} = g\rho_0(1 - \alpha_T T)z_i \tag{3}$$

Motion is driven by the heat escaping from the interior. The energy equation governs the evolution of the temperature in response to advective transport of heat by the fluid and diffusion of heat through the fluid. For a given fluid element,

$$\dot{T} = \frac{\mathrm{D}T}{\mathrm{D}t} = -(\kappa T_{,i})_{,i} + Q(t) \tag{4}$$

where κ is the thermal diffusivity of the material, and $Q(t)$ is a source term attributed to decay of radioactive materials within the Earth.

2.1 Viscosity of Mantle Materials on Geological Timescales

The viscosity of the mantle at long timescale is known to be a strong function of temperature, pressure, stress, grain-size, composition (particularly water

content). Karato & Wu [12], give the following expression for the deformation of upper mantle material:

$$\eta = \frac{1}{2A} \left(\frac{\mu}{\tau}\right)^{n-1} \left(\frac{h}{b^*}\right)^m e^{\frac{E^*+PV^*}{RT}} \tag{5}$$

where A is a constant, μ is shear modulus, b^* is the Burgers vector, T is temperature, τ is the second invariant of the deviatoric stress tensor (i.e $\tau = \sqrt{\sigma_{ij}\sigma_{ij}/2}$ where σ_{ij} is the stress tensor and σ'_{ij} its deviator), E^* is an activation energy, V^* and activation volume, R is the gas constant, h is the grain size, n is a stress exponent, and m a grain-size exponent. Despite this complexity, the dominant effect on the viscosity from the point of view of the large-scale dynamics of the system is the effect of temperature (e.g. Solomatov [22]). Some anisotropy of material properties is observed in mantle materials due to crystallographic realignment during strain but the effect is not well characterized and may be more important in diagnosing strain than in influencing the deformation itself [20].

Fault Model Failure Criterion

An idealized picture of a geological fault is of a two dimensional discontinuity surface arbitrarily embedded in the unfractured rock. In all but the very near surface regions, it is appropriate to assume that the overburden pressure is sufficient to prevent the fault surfaces separating, and that deformation occurs by frictional sliding in the plane of the fault [1]. If we consider a small planar element of the fault with a normal, **n**, and mutually orthogonal vectors, **s** and **m**, lying in the fault plane. The traction resolved in each of these directions is given by:

$$\sigma_{nn} = n_i n_j \sigma_{ij} \tag{6}$$

$$\sigma_{sn} = s_i n_j \sigma_{ij} \tag{7}$$

$$\sigma_{nm} = n_i m_j \sigma_{ij} \tag{8}$$

If we assume that **s** was chosen parallel to the direction of maximum traction in the fault-plane, then the yield criterion for the fault segment is given by $f = 0$ in

$$f = |\sigma_{sn}| + \tan\varphi\,\sigma_{nn} - c \leq 0 \tag{9}$$

Where φ the friction angle and c is cohesion. It is possible to express the magnitude of the maximum shear traction in the fault plane as

$$\tau_s = |\sigma_{sn}| = \sqrt{\sigma_{ik}\sigma_{il}n_k n_l - \sigma_{nn}^2} \tag{10}$$

without explicitly calculating **s**. We note that τ_S is invariant with respect to changes of the pressure p so that $\tau_S(\sigma_{ij}) = \tau_S(\sigma'_{ij})$, where σ'_{ij} is the deviatoric stress tensor.

Continuum Failure Criterion

The previous model applies to a fault which is already established independently of the prevailing stress field and has a length scale which is large with respect to the system as a whole. This description is only appropriate for the largest few faults in any system. We also assume that there are very many faults at smaller scales which can be represented by a continuum approximation. The continuum approximation rests upon the assumption that, at the small scale, all orientations of incipient faults are present. For any given stress field, we can then assume that there is at least one incipient fault within every element of the material which is oriented in such a way that it fails earlier than any other fault and begins to grow. For a point in the material we consider the plane which contains the minimum (here most compressive) and maximum principal stresses (σ_I and σ_{III}). Resolving the stress onto a fault oriented at an angle θ measured positive counterclockwise to the σ_{III} direction yields

$$\sigma_{nn} = \frac{1}{2}(\sigma_I + \sigma_{III}) + \frac{1}{2}(\sigma_I - \sigma_{III})\cos(2\theta) \tag{11}$$

$$\sigma_{sn} = \frac{1}{2}(\sigma_I - \sigma_{III})\sin(2\theta) \tag{12}$$

Substituting into the yield criterion (9) gives:

$$\sigma_I - \sigma_{III} = \frac{\tan\varphi\frac{\sigma_I+\sigma_{III}}{2} + c}{\sin(2\theta) - \tan\varphi\cos(2\theta)} \tag{13}$$

In the early theories of shear failure and shear banding it was assumed that failure takes place on spontaneously forming rupture planes or shear bands which are oriented such that the stress difference on the left hand side of (13) is a minimum (see Brady and Brown [3] for a derivation close to the spirit of Coulomb's (1776) derivation). It is then simple to compute $d(\sigma_I - \sigma_{III})/d\theta$ to find the value of θ_B which minimizes the differential stress required for failure to be

$$\theta_B = \pm\arctan(\tan^{-1}\varphi) = \mp(\frac{\pi}{4} + \frac{\varphi}{2}) \tag{14}$$

Replacing θ by θ_B in (13) gives

$$\frac{\sigma_I - \sigma_{III}}{2} = -\sin\varphi\frac{\sigma_I + \sigma_{III}}{2} + c\cos\varphi \tag{15}$$

In a pristine material we expect faults to form at an angle between $22.5°$ and $45°$ to the most compressive principal stress direction. In the Earth ($\tan\varphi \leq 1$) this means that we expect steep faults to form in extensional environments (**s** close to the direction of gravity) and shallow faults to form in compressive environments (**s** close to orthogonal to the direction of gravity). The orientations (14) can be used to define a curve-linear system of coordinates within the plastic zone of a boundary value problem. The coordinate

lines are the so called static characteristics (see Hill [10] for an outline of the method of characteristics). The static characteristics do not necessarily coincide the orientation of macroscopic shear bands (see the pioneering paper by Rudnicki and Rice [21] and Vardoulakis and Sulem [25] for an outline in the context of geomechanics including experiments).

Flow Rule for Plasticity Model

The yield criterion provides a limit on the acceptable stress states in the material. A corresponding flow rule is needed to determine the manner in which the material deforms when the yield stress is reached. The incompressible fluid assumption which we made in formulating the mantle convection problem is a severe constraint on the possible flow rules. In the theory of plasticity one assumes flow rules of the form

$$\mathbf{D}^p = \dot{\gamma}^p \frac{\partial g}{\partial \sigma} \tag{16}$$

Where $\dot{\gamma}^p$ is the equivalent plastic strain rate and g is the so called plastic potential and $\mathbf{D}^p$ is the plastic part of the stretching; here we assume that the total stretching can be decomposed into a viscous and a plastic part. Elastic strains are assumed as insignificant for the problems considered here. The incompressibility constrain is satisfied if g depends on the deviatoric stress only. Apart from that, g depends on the stress invariants according to the symmetry of the material and possibly on other state variables such as temperature. The standard choice for g in connection with a yield criterion of type (9) or (15) with $\theta = \pm \theta_B$ is $g = \tau_S(\theta = \pm \pi/4) = \sqrt{(\sigma_{11} - \sigma_{22})^2/4 + \sigma_{12}^2}$.

Closer to the implicitly made assumption that upon yielding, plastic deformation consists in frictional sliding on two, possibly simultaneously active sets of thin parallel bands [5] is the following choice of the flow rule:

$$\mathbf{D}^p = \dot{\gamma}_a^p \frac{\partial \tau_S^a}{\partial \sigma} + \dot{\gamma}_b^p \frac{\partial \tau_S^b}{\partial \sigma} \tag{17}$$

where $\tau_S^a = \tau_S(\theta = \pi/4 + \varphi/2)$ and $\tau_S^b = \tau_S(\theta = -\pi/4 - \varphi/2)$ and $\dot{\gamma}_a^p \geq 0$, $\dot{\gamma}_b^p \geq 0$.

We shall concentrate on shear banding processes on a scale involving the lithosphere as well as parts of the underlying asthenosphere. Shear banding may be triggered by the structural non-symmetry of the constitutive equations due to the simultaneous pressure sensitivity of the yield criterion and the assumed incompressibility and/or due to some form of strain softening. In the application we will consider softening of the friction angle and the cohesion. In these applications we adopt a simplified form of the constitutive model where we assume that only one of the two glide mechanisms is active. In this case upon continuing yielding the material deforms like a transversely anisotropic medium of the type proposed by Mühlhaus *et al* [19, 18].

To account for the anisotropic nature of the material, locally transverse-isotropic viscous material is characterised by two effective viscosities, η and η_S, where η is the conventional viscosity and η_S is introduced as a shear viscosity applicable for flow along a layer. The isotropic part of the stretching is then corrected by the Λ_{ijkl} tensor:

$$\sigma_{ij} = 2\eta D_{ij} + 2\left(\eta_S - \eta\right)\Lambda_{ijkl}D_{kl} - p\delta_{ij} \tag{18}$$

where

$$\Lambda_{ijkl} = {}^1\!/_2\left(n_i n_k \delta_{lj} + n_j n_k \delta_{il} + n_i n_l \delta_{kj} + n_j n_l \delta_{ik}\right) - 2n_i n_j n_k n_l$$

and $\mathbf{n}$ is a normal surface vector defining the orientation of the material layering known as the *director*. The inverse form of the constitutive model (18) reads [18]:

$$D_{ij} = \frac{1}{2\eta}\sigma'_{ij} + \left(\frac{1}{2\eta_S} - \frac{1}{2\eta}\right)\Lambda_{ijkl}\ \sigma'_{kl} \tag{19}$$

We also note the relationship:

$$\tau_S = \sqrt{1/2\Lambda_{ijkl}\sigma_{ij}\sigma_{kl}} \tag{20}$$

Since we consider only one slip system we do not need subscripts anymore and designate the equivalent strain rate of the active glide system as $\dot{\gamma}^p$. Comparing (17) and (19) we find the following expression for the shear viscosity η_S:

$$2\eta_S = 2\left(\frac{1}{\eta} + \frac{\dot{\gamma}^p}{\tau_S}\right)^{-1} = \frac{2\eta(\dot{\gamma} - F/\eta)}{\dot{\gamma}}, \qquad \dot{\gamma} = \frac{\partial \tau_S}{\partial \sigma_{ij}}D_{ij} \tag{21}$$

where

$$F = \left(\frac{\partial \tau_S}{\partial \sigma_{ij}} + \tan\varphi\frac{\partial \sigma_{nn}}{\partial \sigma_{ij}}\right)\sigma_{ij}^{\text{vis}} - c, \qquad \sigma_{ij}^{\text{vis}} = 2\eta D_{ij} - \delta_{ij}p \tag{22}$$

Thus:

$$2\eta_S = \frac{-\tan\varphi(2\eta n_k n_l D_{kl} - p) + c}{\dot{\gamma}} \tag{23}$$

The denominator of (23) is the total shear strain rate on the active glide system.

Failure History, Strain Softening and Healing

We now consider a possible history dependency of the mechanical parameters of the glide planes and the effect of deformation on the orientation of the failure planes; we also wish to consider the possibility of simple healing (annealing) of the glide planes or shear bands once de-activated.

Before addressing the above items we note that although our models bares some superficial similarities with the micromechanics based crystallographic

slip theories for metals [4], the present model is very different. We neglect elastic deformations, vacancies and interstitials, the main carriers of the viscous part of the deformation are assumed to diffuse freely through the lattice without affecting the plastic part of the deformation. An intermediate configuration as assumed in elasto-plasticity does not exist in the present case. The glide planes are considered either as shear fractures or in the plasticity case as macroscopic strain localizations usually encompassing multiple grains. Plasticity becomes relevant at greater depth below the top 30 kilometres at large pressures and high temperatures. In this case, the pressure sensitivity (angle of friction) usually disappears. If not, the formal description is analogous to that of fractures. The question then arises as to how the glide planes are affected by deformation and stress rotation. One possibility is to treat the glide planes as embedded in the plastic deformation as described by the history of the inelastic velocity gradient $\mathbf{L}^p$. However, experience with fixed smeared crack models demonstrates that these models tend to cause stress locking, i.e. an artificial build-up of shear stresses along the crack. In the smeared crack model the stress locking was overcome by co-rotating the cracks with the principal stress axes. This is very simple indeed and an analogous approach is adopted here. The glide planes are always oriented relative to the principal stress axes as defined by the mobilized angle of friction φ in relationship (14). In metal plasticity the orientation of the slip planes are constant with respect to the intermediate configuration.

We assume that strain hardening/softening and healing can be described by means of the following relative strain measure:

$$\gamma_{rel}^p = \int \left(\dot{\gamma}^p - \theta \frac{\tau_S}{\eta} \right) \mathrm{d}t \quad , \quad \gamma_{rel}^p \geq 0 \tag{24}$$

In (24) $0 < \theta < 1$ is a dimensionless temperature-dependent healing parameter. Given that the most likely micro-structural features that give rise to shear bands are dislocations, the healing or annealing processes usually involve movement of vacancies (maybe interstitials) to these dislocations which will rearrange themselves into lower energy configurations such as sub-grain structures. The extent of this rearranging process depends on the density of dislocations and the temperature at which the "healing" occurs. The healing is usually considered at a two stage process involving (a) recovery and (b) re-crystallization. Since both processes may occur during deformation itself, the term dynamic can be applied to both processes. Details on the physics of recrystallisation and annealing can be found in Humphreys and Hatherly [11]. Another healing mechanism is associated with fluid flow along channels in grain boundaries and flow in microcracks; this mechanism is several orders of magnitude faster than having vacancies diffuse along such crystalline defect structures as dislocations, dislocation substructures and intact grain boundaries.

The relationship (24) is assumed to hold even if the shear band is not active, i.e. $\dot{\gamma}^p = 0$. The parameter γ_{rel}^p is not a state parameter but a measure

to quantify the relative effect of creation and annihilation of inelastic struc-
tures (e.g. shear bands) caused by plastic deformations chosen for heuristic
reasons.

During the actual calculation, we iterate to determine the distribution of
particles which are currently yielding, we consider first whether each particle
has failed in a previous time step and test to see if it will fail given the
updated stress distribution. In 3D, the slip direction is assumed to lie in
the failure plane in the direction of maximum resolved shear stress. The
friction coefficient and/or the cohesion for the material points which have
failed weaken as relative slip (24) accumulates during yielding. If a material
point has failed in the past but changes in the ambient stress field mean
that it is no longer yielding, then the history parameter (24) decreases until
$\gamma_{rel}^p = 0$.

The cohesion and/or friction coefficient are softened according to

$$c(\alpha) = \alpha c(0) + (1 - \alpha)c(1) \quad \text{and} \tag{25}$$

$$\tan(\phi(\beta)) = \beta \tan(\phi(0) + (1 - \beta) \tan(\phi(1)) \tag{26}$$

where $\alpha = \min(1, \gamma_{rel}^p / \gamma_0^c)$ and $\beta = \min(1, \gamma_{rel}^p / \gamma_0^\phi)$.

3   Numerical Strategies

3.1   Moving Integration Points

The constitutive model described above has been implemented into a La-
grangian integration point finite element code [15]. The method uses a stan-
dard mesh to discretize the domain into elements. The shape functions in-
terpolate node points in the mesh in the usual fashion and are used to com-
pute derivatives of nodal variables. Material property variations, and history
variables such as failure plane orientation and failure history are stored on
integration points which are also material points of the fluid. The problem is
formulated through the usual FEM weak form to give an integral equation
which can then be decomposed to a series of element integrals and through
the usual Galerkin discretization procedure, give element stiffness matrices,
$\mathbf{K}^E$:

$$\mathbf{K}^E = \int_{\Omega_E} \mathbf{B}^T(\mathbf{x})\mathbf{C}(\mathbf{x})\mathbf{B}(\mathbf{x}) \, \mathrm{d}\Omega \tag{27}$$

We replace the continuous integral by a summation

$$\mathbf{K}^E = \sum_p w_p \mathbf{B}_p^T(\mathbf{x}_p)\mathbf{C}_p(\mathbf{x}_p)\mathbf{B}_p(\mathbf{x}_p) \tag{28}$$

Here the matrix $\mathbf{B}$ consists of the appropriate gradients of interpolation
functions which transform nodal point velocity components to strain-rate

pseudo-vectors at any points in the element domain. $\mathbf{C}$, the constitutive operator corresponding to (18), is composed of two parts $\mathbf{C} = \mathbf{C}_{iso} + \mathbf{C}_{aniso}$. In standard finite elements, the positions of the sample points, $\mathbf{x}_p$, and the weighting, w_p are optimized in advance. In our scheme, the $\mathbf{x}_p$'s correspond precisely to the Lagrangian points embedded in the fluid, and w_p must be recalculated at the end of a timestep for the new configuration of particles.

3.2   Scripting of Boundary Value Problems

The toolkit *Escript* [9] has been applied to obtain the results relating to planetary scale mantle convection. *Escript* provides a scripting interface in which specific differential problems are stated to parallelised computational kernels, shielding the user from low-level parallel development. Of particular interest, the *"Finley"* FEM computational kernel has been used within *Escript* to solve the constitutive equations of section 2. A brief overview of *Finley* and its FEM implementation is presented in this section.

To use *Finley*, the Data module is used to transform an initial boundary value problem (IBVP) into a sequence of linear BVPs to be solved at each time step. The linear BVP can then be provided to *Finley* to assemble a stiffness matrix associated with a given unstructured domain using a discretisation based on the standard variational formulation appropriate for the supplied mesh and selected element type. The linear BVP is then provided to *Finley* to assemble a stiffness matrix associated with a given unstructured mesh using a discretisation based on the standard variational formulation.

For an unknown vector function u, the PDEs of a BVP are provided to *Finley* through the specification of the coefficients of the following templated form in tensorial notation:

$$-(A_{ijkl}u_{k,l})_{,j} - (B_{ijk}u_k)_{,j} + C_{ikl}u_{k,l} + D_{ik}u_k = -X_{ij,j} + Y_i \qquad (29)$$

The tensorial coefficients A, B, C, D, X and Y are functions of their location in the physical domain. For example, to solve equation (3) for velocity, the identification of like terms with (29) reveals it is necessary to provide *Finley* with A, X, and Y only.

In a similar manner, *Finley* provides a system of implicit (natural) boundary conditions and explicit Dirichlet boundary conditions as given by the respective systems:

$$n_j(A_{ijkl}u_{k,l} + B_{ijk}u_k) + d_{ik}u_k = n_jX_{ij} + y_i \ \text{ on } \Gamma^N \qquad (30)$$

$$u_i = r_i \ \text{ on } \Gamma^D \qquad (31)$$

where n denotes the outer boundary normal, and A, B and X are as previously defined. Here, d and y are coefficients defined on the natural boundary Γ^N while r is a function defined on the Dirichlet boundary Γ^D. The linear BVP defined by equations (29)–(31) is referred to as the *Finley Boundary*

Value Template (FBVT). Finally, a general form of the FBVT for the case of a steady BVP with a single differential equation in a scalar unknown also exists.

4   The Level Set Method

We use the level set method to track the moving and deforming interface between lithosphere and mantle in subduction models. It is a part of Escript/Finley. This method is based upon an implicit representation of the interface by a smooth function . The function usually has the form of a signed distance to the interface, whereby the zero level curve or surface represents the actual interface between the fluids. The field equations are solved on an Eulerian mesh. The parameters are stored as tables, their value depending upon which side of the interface they are located. The distance function is updated during the simulation by solving the equation of motion using the velocity field calculated previously. The level set method is particularly well suited for two or three dimensional problems with strong topological changes such as breaking or merging as well as the formation of corners and cusps. The level set algorithm works as follows: A scalar function, ϕ is initialised on an Eulerian grid as a signed-distance function with respect to the interface. The values of the parameters are then calculated, depending upon the sign of ϕ. The governing equations can be solved using these parameters, resulting in a velocity field. At each time step, the function ϕ must be updated, according to the velocity field. This is done by solving the "advection equation":

$$\frac{\partial \phi}{\partial t} + \mathbf{v} \cdot \nabla \phi = 0 \tag{32}$$

where $\mathbf{v}$ is the velocity field. Special care must be taken when solving the advection equation and a two step method based on the Taylor-Galerkin procedure is used. For a detailed presentation of this method, we refer the reader to a previous publication by Bourgouin et al. (2006)

5   Examples

5.1   *Shear Banding*

We now consider the extension and compression of a brittle layer which lies above a viscous layer for a range of non-dimensionalised material properties and strain-softening parameters. In each case the deformation is driven by a boundary condition which uniformly stretches or compacts the background mesh (initial size 2.0×1.0) in the horizontal direction only with a velocity of 1.0. The evolving interface geometry and material history is recorded on the
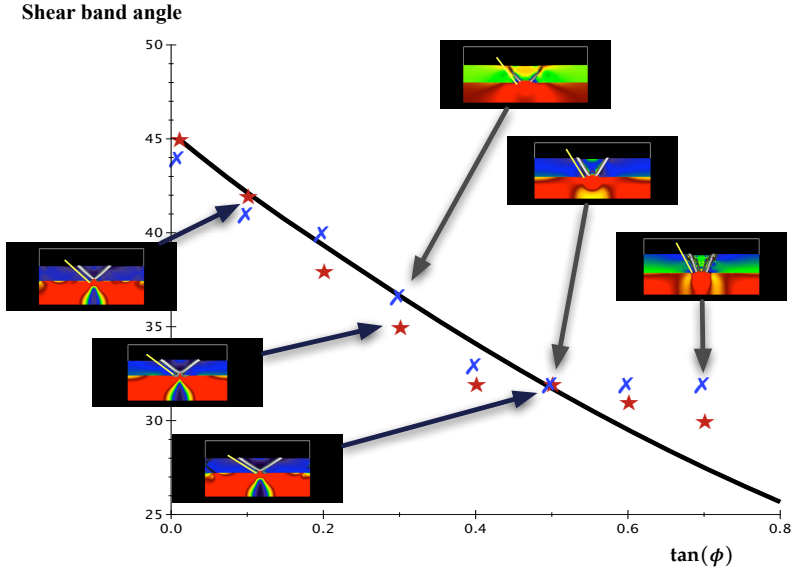
Fig. 1 Shear band formation in compression (stars) and extension (crosses) of a layer of length 2.0, thickness 0.35 with a small notch removed, viscosity $\eta = 10.0$, cohesion 4 (compression) and 15 (extension). The compression/extension velocity is 1.0; the lower layer viscosity is 1.0, the upper layer viscosity is 0.1 and this material is compressible. The ideal orientation of shear bands assuming the principle stress orientations are horizontal/vertical is indicated by the broad white lines on each image.

swarm of particles. A layer of low-viscosity, compressible material is always included in the calculation above the layers of interest to allow the volume change of the domain to be accommodated. In geological models the effect of gravity is always important so we have included this effect. The strength of gravitational acceleration is 10.0 and the density of the layers is 1.0. The shading in the figures represents the second invariant of the stress tensor plotted between 0 and 10 in the top layer and 0 and 1 in the lower layer.

In Figure 1, a brittle layer of thickness 0.35, viscosity 10.0, and cohesion 4 (compression), 15 (extension) lies above a purely viscous layer of viscosity 1.0. The strain softening parameter, γ was 0.1 for all six models shown, and the minimum value of the cohesion was 1.0 at this reference strain. A narrow notch of material in the brittle layer was removed (replaced by material of the lower layer) to provide an initial stress concentration which encourages shear band formation.

In this experiment, the layers were only deformed until the pair of shear bands had developed across the entire layer – total strain of between 2% and 5%. The orientation of these shear bands was then compared with the ideal orientation of the slip planes (assuming that the orientation of the principal

stress directions is not strongly influenced by the shear band formation) which
is indicated in the diagram by the light coloured line. In compression the fit
between the macroscopic shear band orientation and the microscopic material
point slip orientation is very close. In extension the shear bands form at
shallow angles for low values of the cohesion, steeper angles for higher values,
but the agreement between the microscopic slip orientation and the shear
bands is not as good. We attribute this to the fact that at shallow depths
in the layer the gravitational loading is insufficient to keep the fault surfaces
in contact during extension, so that our assumption that all failure occurs
through pure frictional sliding is not valid. Our model does not allow the
possibility of failure in tension and clips the second viscosity to slightly above
zero whenever it would be zero or negative.

5.2 Large Deformation Model

Figure 2 shows the evolution of the deformation when the extension is com-
paratively large. In this model we account for gravitational loading of the
crust. The dimensionless gravitational acceleration is 100, the cohesion is
1.0, and $\tan(\phi)$ is 0.5. The grid resolution was 300×150 elements and the
total extension was 70%. We plotted the upper layer deformation using ini-
tially horizontal stripes of passive markers to indicate the total deformation.
The instantaneous plastic deformation rate was plotted in bright white su-
perimposed on the stripes in the background.

   An initially large number of active shear bands in the upper part of the
brittle layer reduced during the first 1-2% of extension as strain softening
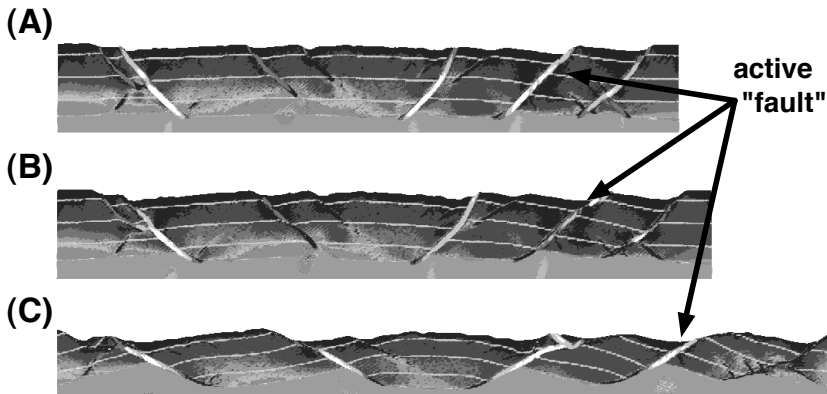

Fig. 2 A model crust with initial random orientations of damage was extended
by 20% (A), 28% (B) and 70% (C). The horizontal stripes in the upper layer are
passive strain markers. Current plastic strain rate is indicated by the intensity of
the white colouring in the shear bands.

within the shear bands allowed them to compete. Throughout the deformation experiment, due to stress transfer from the lower, viscous layer, there are approximately five active shear bands which accumulate significant slip (from a visual inspection of the strain markers).

At the end of the experiment it is possible to see how resilient shear bands have rotated during extension. These are the shear bands which have accumulated significant slip and, consequently, are significantly weaker than surrounding material. This population of shear bands coexists with a second generation which have formed at steep angles in the less deformed blocks, and some old scars of shear bands which were active early in the experiment.

5.3   Subduction

Because of the required higher resolution and numerically more demanding rheology, it has not been possible to include subduction directly into global models. Some subgrid parameterization – like for the phase boundaries in the mantle – would be desirable for subduction. However, despite its importance for the thermal and tectonic evolution of the Earth, recent studies still deal with the fundamental controls of subduction. The current modelling strategy is to isolate specific aspects of subduction zone behaviour in models that are as simple as possible. The following example focuses on the effects of the tear resistance at the subduction zone edges (Hale et al., 2009). It is a geometrical consequence of finite subduction zone length and subduction hinge migration that some edges of subduction zones propagate through the subducting plate (Govers & Wortel, 2005). Continued subduction requires ongoing tearing of the lithosphere. Once established, tear faults are able to propagate as long as subduction continues and the lithospheric strength is less than the slab strength. Otherwise subduction may stall or the slab may break off. Tear propagation is dominated by shear stresses, acting parallel to the fault plane and parallel to the crack front. Such a tearing configuration is also known as Mode 3 Crack in fracture mechanics. The tear fault is most likely to propagate parallel to the direction of rollback, but might also follow pre-existing weak zones. Tearing of the lithosphere is a shallow process. Hence compressibility can be neglected. The density variations driving subduction are mainly due to cooling of the lithosphere. We impose an unstable density stratification as initial condition, rather than calculating it from the energy equation. Although thermal diffusion is present in real subduction, it acts on a longer timescale than advection. We use a simplified model setup (Fig. 3) to gain first-order understanding of resistance to tear propagation on the dynamics and morphology of subduction zones.

The results show the importance of tear resistance for the speed of trench migration and for shaping the final geometry of subduction systems. Figure 4 shows that slab tearing along a weak layer can result in a relatively straight slab hinge shape, while increasing the strength in the weak layer results in the curvature of the hinge increasing substantially. The rollback velocity of the
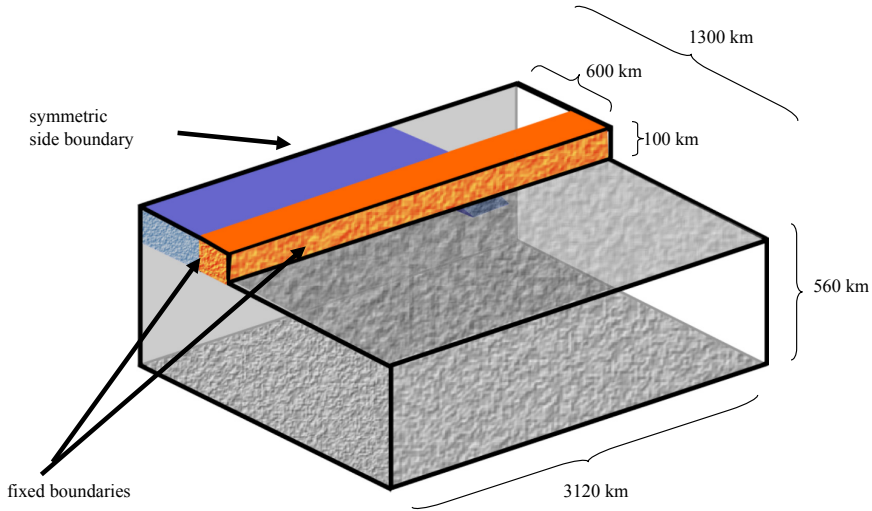
Fig. 3 Our modelling domain is a box, containing a part of a lithospheric plate, with a subducting slab (blue) and the underlying upper mantle. We prescribe a visco-plastic weak zone (orange) and vary its rheological parameters, i.e. the tear resistance.

simulated subduction zones is time-dependent. It reaches 2.5 cm/yr for the fixed weak zone (figure c) and more than 14 cm/yr for the free-slip weak zone. Those values are comparable to the observed range (Schellart et al., 2007). Rollback velocity controls the induced mantle flow, which is also deforming the sinking slabWe used the finite element code eScript/Finley and the level set method to describe the lithosphere to solve this fluid dynamics problem.

5.4   Mantle Convection

Turning to the longest planetary scale we use the temperature-dependent rheology (5) to explore the mechanical conditions underlying the 3 basic types of planetary convection modes, namely stagnant lid, episodic subduction and continuous (Earth-like) convection modes. Viscous deformation is described by a combined Newtonian and power law creep model. The power law viscosity includes a contribution from dislocation glide, a typical power law exponent ($n = 3$) and a contribution from von Mises plastic deformations with temperature independent coefficients and a large exponent ($n = 15$). The effective viscosity is given by:

$$\frac{1}{\eta_{eff}} = \frac{1}{\eta_N} + \frac{1}{\eta_N \left(\dfrac{\tau}{\tau_0}\right)^{1-n}} + \frac{1}{\eta_Y \left(\dfrac{\tau}{\tau_Y}\right)^{1-n_p}} \tag{33}$$
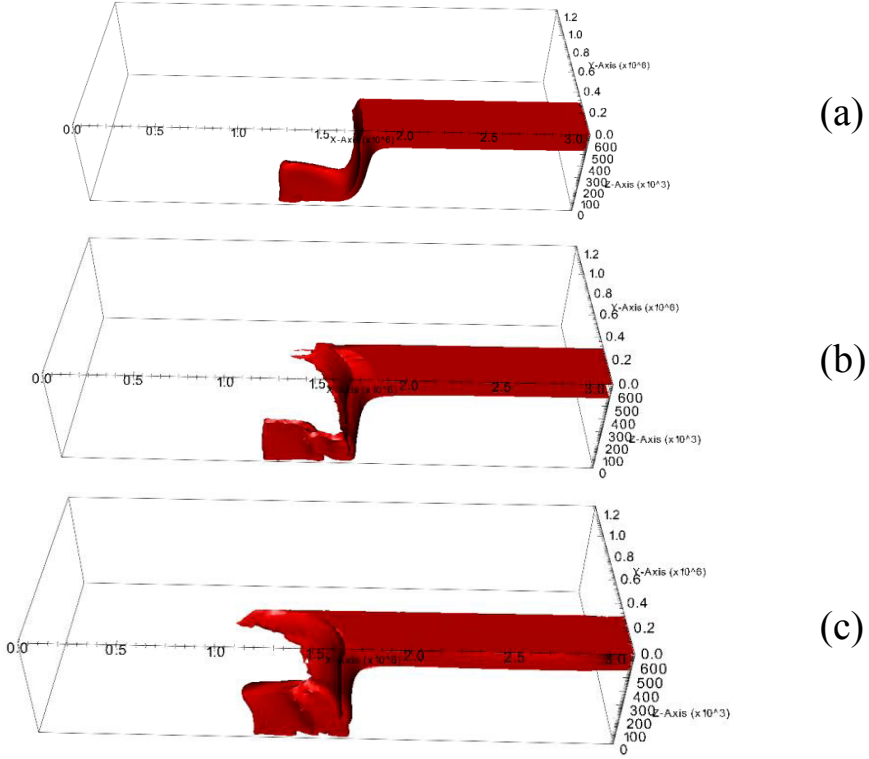
Fig. 4 Snapshots showing the subducting lithosphere after the slab hinge has rolled-back a distance of 500 km. All simulations have a yield strength of 100MPa for the plate and a density difference between plate and mantle of $= 69$ kg m^{-3} (a) Free slip in the weak zone (yield stress $= 0$ MPa);(b) Yield stress in the weak zone $=$ 25 MPa (c) Fixed boundary in the weak zone.

where η_N is the temperature dependent Newtonian viscosity, η_Y is a reference viscosity for plastic deformation, τ is the second deviatoric stress invariant, τ_0 is the reference transition stress, and τ_Y is the reference yield stress invariant. For η_N we assume the Arrhenius relationship:

$$\eta_N = \eta_{N0}e^{\frac{AT_M}{T}} \qquad (34)$$

where $AT_M = E^*+PV^*/R$, T_M is the pressure dependent melting temperature, A is a positive constant (distinct from that used in (5)) and η_{NO} is the viscosity as $T \to \infty$.

In the convection study of section 5.4 we ignore the pressure dependence of T_M in the Arrhenius relation. The main emphasis in the study will be on the role of elasticity, power law creep and plasticity on the emergence of different

styles of convection. In the dimensionless formulation we write the Arrhenius relationship of (34) as follows [23]:

$$\eta_{NO}e^{\frac{2\hat{A}}{3}}e^{\hat{A}\left(\frac{1}{1+T}-\frac{2}{3}\right)} = \eta_{ref}e^{\hat{A}\left(\frac{1}{1+T}-\frac{2}{3}\right)} \tag{35}$$

Here, η_{ref} is the reference viscosity used in the definition of the Rayleigh number. This corresponds to a Newtonian viscosity contrast of about 10^5 across the convection cell. In the applications we assume that $\hat{A} = 23$. In the absence of convection, the ratio of the Newtonian viscosity to η_{ref} varies slowly due to temperature change in the lower half of the cell, from 1 in the middle to 0.022 on the bottom and rapidly in the upper half from 1 to 2087 on the top.

In the formulation of the constitutive model we make the standard assumption that the symmetric part of the velocity gradient, the so called stretching, is the sum of elastic, and a visco-plastic part, i.e.:

$$D_{ij} = D_{ij}^{\mathrm{e}} + D_{ij}^{\mathrm{vp}} \tag{36}$$

We assume incompressible flow so that $D_{ii} = v_{i,i} = 0$. According to (33) the visco-plastic stretching is defined as:

$$D_{ij}^{\mathrm{vp}} = \frac{\sigma_{ij}'}{2\eta_{eff}} \tag{37}$$

and for the elastic part we assume:

$$D_{ij}^{\mathrm{e}} = \frac{\dot{\sigma}_{ij}^{J'}}{2\mu} \tag{38}$$
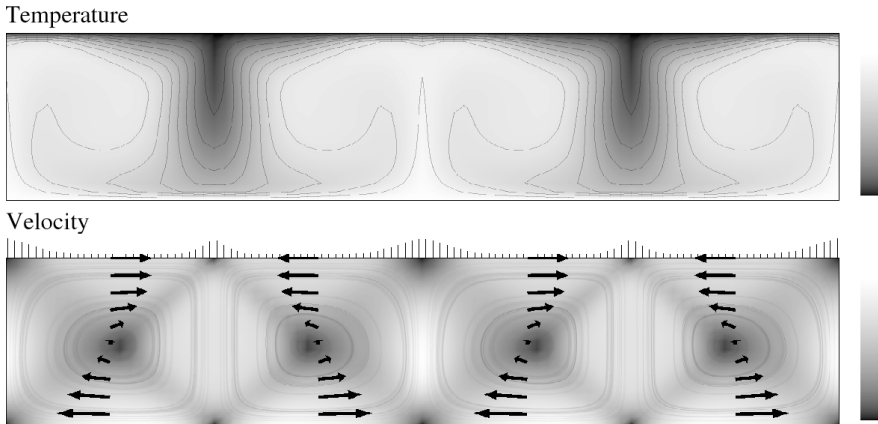
Temperature

Velocity

Fig. 5 Typical temperature and velocity distributions for episodic convection at a maximum of the Nusselt number (refer to Figure 8)

where μ is the elastic shear modulus and $\dot{\sigma}^J{}_{ij}$ is the Jaumann stress rate (see Kolymbas and Herle [13] and Mühlhaus and Regenauer-Lieb [17] for recent discussions and objective stress rate comparisons). The Jaumann stress rate is related to the material stress rate as:

$$\dot{\sigma}^J{}_{ij} = \sigma_{ij,t} + v_k \sigma_{ij,k} - W_{ik}\sigma_{kj} + \sigma_{ik}W_{kj} \tag{39}$$

where W_{ij} is the non-symmetric part of the velocity gradient.

The temperature dependence of the viscosity was given by (35), resulting in a viscosity ratio from the cold to the hot boundary of 10^5 due to temperature variation alone. More extreme viscosity contrasts can be easily considered in the present formulation because the upper limit for the effective dimensionless viscosity is set by the dimensionless elastic shear modulus and the time increment $\mu t_D \delta t / \eta^*$. We assume $Ra = 10^4$, $\tau_0 = 0.866 \times 10^{5/2}$, $\tau_Y = 3\tau_0$, ideal plasticity ($\tau_Y =$ constant) and $\mu t_D / \eta^* = 10^4$ In the simulations we use the power law plasticity model with $n_Y = 15$ and $\eta_Y = \eta_N O$. The initial temperature distribution was

$$T = \frac{1}{10}\sin(x_2\pi)\cos(x_1\pi) + (1 - x_2) \tag{40}$$

The basic modes of convection applicable to a cooling planet, such as stagnant lid, episodic resurfacing and mobile lid convection have been reproduced with the non-linear viscoelastic approach and are shown in figures 5, 6, and 7 respectively. The vertical spikes on top of the velocity streak-line plot in each of the subfigures represent the relative magnitudes of the horizontal cold boundary velocities: larger spikes represent lower velocities, and smaller spikes represent higher velocities. A comparison between the Nusselt numbers for the stagnant, episodic and mobile lid cases is shown in figure 8.
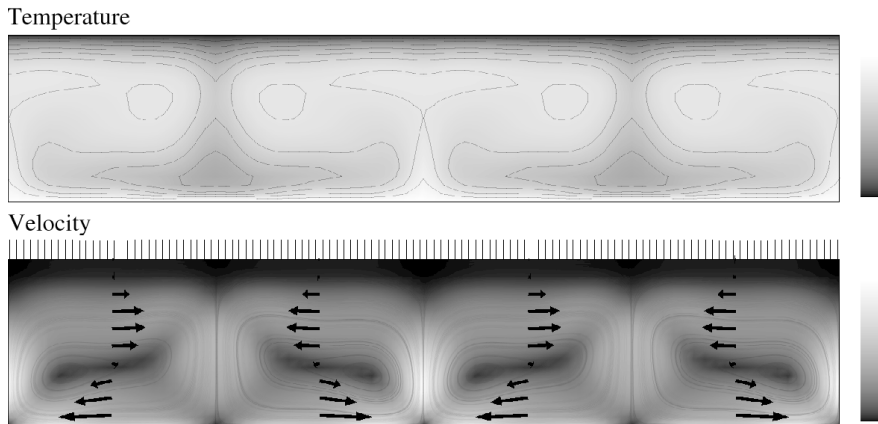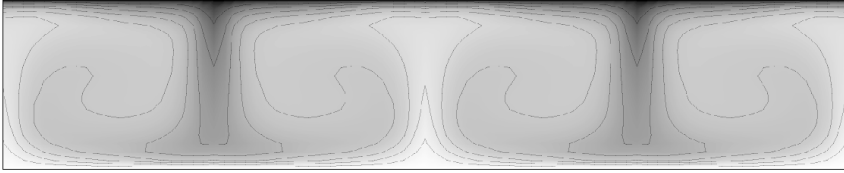
Temperature

Velocity

Fig. 6 Typical temperature and velocity distributions for episodic convection at a minimum of the Nusselt number (refer to Figure 8)
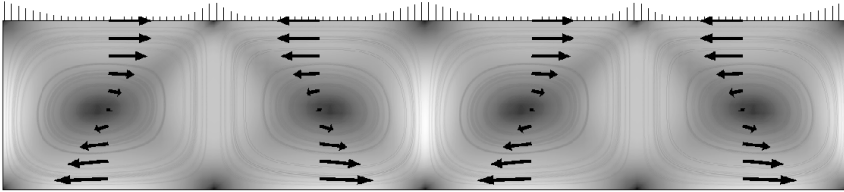
Temperature

Velocity

Fig. 7 Typical temperature and velocity distributions at steady state for mobile lid convection. For mobile lid convection, significant parts of the top layer move like rigid bodies.
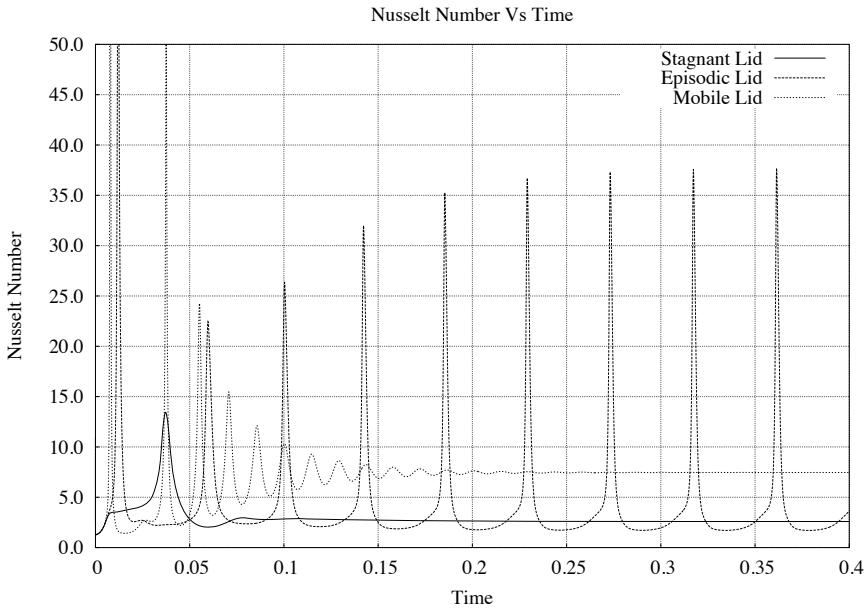

Fig. 8 A comparison of Nusselt numbers for stagnant-lid (lowest with steady state) episodic and mobile lid convection. Here the yield stress τ_y is respectively a factor of 3, 6 and 9 times the transition stress $\tau_0 = 0.866 \times 10^{25}$ (i.e. the transition from Newtonian-Power law creep). The dimensionless shear modulus is 10^4. An Arrhenius relation describes the temperature dependence of creep with a viscosity contrast across the layer of 10^5. The power law exponents are $n = 3$ and $n = 15$ (dislocation glide and plastic deformation respectively).

A slight but noticeable shift in parameter values and validity fields for cases including elasticity has been recorded. In addition, the buffering action of elasticity permits solutions to extreme viscosity variations and introduces long-range interactions. This results in an ordering and stabilization of patterns of convection at high Rayleigh numbers, replacing smaller-scale turbulence by larger planetary-scale re-mobilization.

6   Conclusions

The plasticity algorithm described in this paper addresses a prominent problem in geodynamics: how to model the brittle deformation of the uppermost lithosphere which occurs when mantle convection deforms the continents at the same time as modelling the underlying fluid convection which drives the surface deformation. The formulation has been developed from a mathematical description of fluid flow which is inherently capable of modelling thermally driven convection.

By locally satisfying the failure criterion for frictional sliding and adopting the assumption that deformation initially occurs along the static characteristics, we have generated macroscopic shear bands aligned with the static characteristics of the global stress field. A strain softening model based on the accumulated slip at failed material points is required for localization to occur.

In a simple extension experiment, the shear bands interact to generate geologically plausible patterns of deformation including rotated fault blocks and multiple generations of faults.

We have also outlined a formulation for visco-elastic convection based on a combined Newtonian and power law rheology; the effect of plastic yielding is considered by an additional power law term with a high ($n = 15$) power law coefficient (Equation (33)). The model is valid for studying the geodynamics of mantle convection amongst other problems. The nonlinear equations of motion are solved incrementally based on a consistent tangent formulation producing second order accurate results so that iterations within each time step are not necessary in most cases. In Moresi and Solomatov [16] and Tackley [24], plastic yielding is considered by introducing an upper limit to the viscosity given by the ratio of the yield stress and the equivalent viscous strain rate. Since the strain rate strain rate at the current time is unknown, an initial estimate has to be based on the strain rate from the last time step producing first order accurate results; hence a time consuming, iterative approach is necessary. The iterative approach is usually more time consuming than the present incremental approach with occasional iterative reduction of residuals. In the iterative approach the constitutive operator is more sparse than in the consistent incremental approach, which sometimes can be used to advantage.

The convection problem with strongly temperature dependent viscosity has some unique characteristics: the strains in much of the system are very

large, necessitating a fluid-dynamics formulation, yet the relaxation time in the cool thermal boundary layer is significant compared to the characteristic time associated with fluid flow. In the bulk of the fluid the relaxation time is small compared to the time taken for convective features to evolve due to the much lower viscosity of the warm fluid.

Because elastic stresses in the strongly convecting part of the system relax rapidly, the introduction of elasticity does not produce a qualitative change to the stagnant lid convection regime (see Solomatov [22]). In episodic and mobile lid regimes, there is a competition between the build-up of stresses in the cool lid, and the stress-limiting effect of the yield criterion. The introduction of elastic deformation does not quantitatively influence this balance either, although we do expect a difference in the distribution of stresses in the lid, which explains the variation in the onset of overturns and their increasing frequency which we observed as the elastic shear modulus was reduced.

The presence of an elastic deformation mechanism also allows significant deformation of the highly viscous lid with considerably lower viscous energy-dissipation rates. This is reflected in the lower energy dissipation during episodic overturns which we observed by integrating the system Nusselt number. In the Earth this effect may be important in subduction zones where prediction of dissipation rates due to slab bending is un-physically large. We observed a breakdown in the highly regular boundary layer overturn time when moving from a perfectly harmonic initial condition to a non-harmonic initial condition. This is similar to the results of Moresi and Solomatov [16], who noted for the purely viscous case that the regularity of the episodic regime was an artifact of the small convection domains. Once we break the perfect symmetry of the convection pattern, the evolution also becomes significantly more time-dependent.

We note, finally, keeping our goal of a unified planetary dynamics model in mind, that the two formulations can be merged as the orthotropic constitutive law can be inverted from the stress/strain-rate relationship of (18) to that of (19) and substituted into (37).

References

[1] Barr, A.H.: Superquadrics and angle-preserving transformations. IEEE Computer Graphics and Applications 1(1), 11–23 (1981)

[2] Bird, P., Kong, X.: Computer simulations of california tectonics confirm very low strength of major faults. Geol. Soc. Am. Bull. 106, 159–174 (1994)

[3] Brady, B.H.G., Brown, E.T.: Rock Mechanics. George Allen and Unwin., London (1985)

[4] Bronkhorst, C.A., Kalidindi, S.R., Anand, L.: Polycrystalline plasticity and the evolution of crystallographic texture in fcc metals. Phil. Trans. Royal Soc. A 341, 443–477 (1992)

[5] de Josselin de Jong, G.: The double sliding free rotating model for granular assemblies. Geotechnique 21, 155–163 (1971)

[6] England, P., Houseman, G.: Role of lithospheric strength heterogeneities in the tectonics of tibet and neighbouring regions. Nature 315, 297–301 (1985)

[7] England, P., Houseman, G., Sonder, L.: Length scales for continental deformation in convergent, divergent and strike-slip environments: Analytical and approximate solutions for a thin viscous sheet model. J. Geophys. Res. 90, 3551–3557 (1985)

[8] England, P.C., Houseman, G.A.: The mechanics of the tibetan plateau. Philos. Trans. R. Soc. Lond. Ser. A-Math. Phys. Eng. Sci. 326, 301–320 (1988)

[9] Gross, L., Bourgouin, L., Hale, A.J., Muhlhaus, H.-B.: Interface modeling in incompressible media using level sets in escript. Physics of the Earth and Planetary Interiors 163, 23–34 (2007)

[10] Hill, R.: The Mathematical Theory of Plasticity. Oxford University Press, Oxford (1998)

[11] Humphreys, F.J., Hatherly, M.: Recrystallization and related annealing phenomena. Pergamon Press, U.K. (1995)

[12] Karato, S., Wu, P.: Rheology of the upper mantle - a synthesis. Science 260, 771–778 (1993)

[13] Kolymbas, D., Herle, I.: Shear and objective stress rates in hypoplasticity. Int. J. Numer. Anal. Methods Geomech. 27, 733–744 (2003)

[14] Kong, X., Bird, P.: Thin-shell finite- element models with faults. In: Yin, A., Harrison, T.M. (eds.) The Tectonic Evolution of Asia, pp. 18–34. Cambridge University Press (1996)

[15] Moresi, L., Dufour, F., Muhlhaus, H.B.: A lagrangian integration point finite element method for large deformation modeling of viscoelastic geomaterials. Journal of Computational Physics 184, 476–497 (2003)

[16] Moresi, L.N., Solomatov, V.S.: Mantle convection with a brittle lithosphere: thoughts on the global tectonic styles of the earth and venus. Geophysicical Journal International 133, 669–682 (1998)

[17] Muhlhaus, H.-B., Regenauer-Lieb, K.: Towards a self-consistent plate mantle model that includes elasticity: simple benchmarks and application to basic modes of convection. Geophys. J. Int. 163(2), 788–800 (2005)

[18] Muhlhaus, H.-B., Dufour, F., Moresi, L., Hobbs, B.: A director theory for viscoelastic folding instabilities in multilayered rock. Int. J. Solids Structures 39, 3675–3691 (2002)

[19] Muhlhaus, H.B., Moresi, L., Hobbs, B., Dufour, F.: Large amplitude folding in finely layered viscoelastic rock structures. Pure and Applied Geophysics 159, 2311–2333 (2002), doi:10.1007/s00024-002-8737-4

[20] Muhlhaus, H.B., Moresi, L., Cada, M.: Emergent anisotropy and flow alignment in viscous rock. Pure Appl. Geophys. 161, 2451–2463 (2004)

[21] Rudnicki, J.W., Rice, J.R.: Conditions for the localization of deformation in pressure sensitive dilatant materials. J. Mech. Phys. Solids 23, 371–394 (1975)

[22] Solomatov, V.S.: Scaling of temperature- and stress- dependent viscosity convection. Phys. Fluids 7, 266–274 (1995)

[23] Tackley, P.J.: Three-dimensional simulations of mantle convection with a thermo-chemical basal boundary layer: D"? Americal Geophysical Union (1998)

[24] Tackley, P.J.: Self-consistent generation of tectonic plates in threedimensional mantle convection. Earth Planet. Sci. Lett. 157, 9–22 (1998)

[25] Vardoulakis, I., Sulem, J.: Bifurcation Analysis in Geomechanics. Blackie Academics and Professional (1995)

[26] Watts, A.B., Bodine, J.H., Ribe, N.M.: Observations of flexure and the geological evolution of the pacific basin. Nature 283, 532–537 (1980)

[27] Watts, A.B., Bodine, J.H., Steckler, M.S.: Observation of flexure and the state of stress in the oceanic lithosphere. J. Geophys. Res. 85, 6369–6376 (1980a)

[28] Zhong, S.J., Gurnis, M.: Controls on trench topography from dynamic-models of subducted slabs. J. Geophys. Res.-Solid Earth 99, 15683–15695 (1994)

[29] Zhong, S.J., Gurnis, M.: Towards a realistic simulation of plate margins in mantle convection. Geophys. Res. Lett. 22, 981–984 (1995)

[30] Zhong, S.J., Gurnis, M.: Mantle convection with plates and mobile, faulted plate margins. Science 267, 838–843 (1995)

[31] Zhong, S.J., Gurnis, M.: Interaction of weak faults and non-newtonian rheology produces plate tectonics in a 3d model of mantle flow. Nature 383, 245–247 (1996)

[32] Zhong, S.J., Gurnis, M., Moresi, L.: Role of faults, nonlinear rheology, and viscosity structure in generating plates from instantaneous mantle flow models. J. Geophys. Res.-Solid Earth 103, 15255–15268 (1998)